

Cite this: *Mater. Adv.*, 2022,
3, 7098

Crystal actuation switching by crystal thickness and light wavelength†

Shodai Hasebe,^a Yuki Hagiwara,^a Kazuya Hirata,^a Toru Asahi^{ab} and Hideko Koshima^{*b}

Photomechanical molecular crystals have been developed over the past two decades, and actuation switching is an important requirement for their practical application. In this study, we developed a method for actuation switching of the isomorphous crystals of two salicylideneaniline derivatives, where bending direction and speed are controlled by crystal thickness and light wavelength. Upon ultraviolet (UV) light irradiation of its top face, a thin crystal bends toward the light source through photoisomerisation. In contrast, a thick crystal bends away rapidly through the photothermal effect. Slightly thick crystals exhibit two-step bending that involves a combination of these two mechanisms, first bending away quickly through the photothermal effect and then bending toward the light source through photoisomerisation. The bending motions of thin and slightly thick crystals switch to two-step bending and bending away, respectively, upon UV light irradiation of the side face. Visible light irradiation alters the bending motions of thin and slightly thick crystals to no significant bending and bending away, respectively. These results provide a novel, convenient, and useful approach for switching the crystal bending direction and speed, thereby expanding the versatility of molecular crystals as actuation materials.

Received 15th July 2022,
Accepted 28th July 2022

DOI: 10.1039/d2ma00825d

rsc.li/materials-advances

Introduction

Mechanically responsive materials, which exhibit macroscopic motion in response to external stimuli such as light, heat, and electricity, have been studied extensively from the perspectives of basic research and practical application.¹ Among these external stimuli, light is useful in that its properties (*e.g.*, wavelength, intensity, and polarisation) can be optimised for specific requirements at high spatial and temporal resolution, as well as under remote control.^{2,3} Various light-fuelled materials have been developed within the past two decades; a notable example includes light-responsive liquid crystal polymer networks.^{1–5}

Despite their hard, brittle appearance, molecular crystals exhibit macroscopic deformation upon irradiation with light.^{1,6–11} Compared with polymers, molecular crystals are more advantageous in light-driven actuators and soft robots

because of their higher elastic modulus and stronger output force.⁹ Thus far, various light-fuelled (*i.e.*, photomechanical) crystals that exhibit bending,^{12–28} twisting,^{23,29,30} bending with twisting,^{31,32} curling,³³ rotation,^{34,35} peeling,^{36,37} and jumping^{38,39} have been developed; these characteristics are mainly based on the photoisomerisation (sometimes photodimerisation) of molecules. Recently, we reported rapid bending of molecular crystals through the photothermal effect, in which thermal energy is produced by photoexcitation of a material;⁴⁰ we unveiled that the bending mechanism was driven by a non-steady temperature gradient in the thickness direction.⁴¹ Compared with photoisomerisation, the photothermal effect has several advantages in crystal actuation, including higher speed, greater light wavelength range, and actuation of thicker crystals.⁴¹

To increase the applicabilities of these photomechanical crystals in actuators and soft robotics, there is a need to diversify their mechanical motions. One method for achieving this goal involves utilising polymorphism, in which one type of molecule forms multiple crystalline structures.^{42–44} Another approach involves utilising different crystal actuation mechanisms.^{45–49} Our research group created four motions from different crystal forms of the same molecule by combining two polymorphs (α and β) and two actuation mechanisms (photoisomerisation and the photothermal effect).⁵⁰

Actuation switching is another requirement for the practical application of photomechanical crystals. Among salicylideneaniline crystals, photoisomerisation actuates thin crystals,

^a Graduate School of Advanced Science and Engineering, Waseda University, 3-4-1 Okubo, Shinjuku-ku, Tokyo, 169-8555, Japan

^b Research Organization for Nano & Life Innovation, Waseda University, 513, Waseda Tsurumakicho, Shinjuku-ku, Tokyo, 162-0041, Japan.
E-mail: h.koshima@kurenai.waseda.jp

† Electronic supplementary information (ESI) available: Detailed methods, crystallographic data (CIF and other formats), photoisomerisation properties, photomechanical motions, and movies. CCDC 2178010 and 2178011. For ESI and crystallographic data in CIF or other electronic format see DOI: <https://doi.org/10.1039/d2ma00825d>





Scheme 1 Enol–keto photoisomerization of salicylideneaniline **1**.

whereas the photothermal effect actuates thick crystals;^{41,50} the photoisomerisation mechanism can be induced by ultraviolet (UV) light alone, whereas the photothermal effect mechanism can be induced by both UV and visible light.⁴¹ Therefore, we hypothesised that crystal actuation could be switched by changing the crystal thickness or light wavelength. A previous study reported actuation mode switching in a diarylethene crystal in response to changes in UV light irradiation direction;⁵¹ it may be possible to further control crystal actuation by tuning the light-irradiated face.

In this study, we developed a method to switch the actuation of isomorphous crystals of two salicylideneaniline derivatives, *N*-3,5-di-*tert*-butylsalicylidene-4-chloroaniline (**1a**) and *N*-3,5-di-*tert*-butylsalicylidene-4-bromoaniline (**1b**), in enol form (Scheme 1)⁵² by changing crystal thickness and light wavelength.

Experimental

Preparation of materials

Two compounds, *p*-chlorosalicylideneaniline enol-**1a** and *p*-bromosalicylideneaniline enol-**1b**, were synthesised through the condensation of 3,5-di-*tert*-butylsalicylaldehyde and 4-chloroaniline (**1a**) and 4-bromoaniline (**1b**), respectively, by microwave heating (Monowave 300, Anton Paar, Graz, Austria) for one hour at 150 °C. Single bulk, thick crystals of enol-**1a** and enol-**1b** were prepared by slow evaporation of methanol solutions at ambient temperature under atmospheric pressure. Single micro, thin crystals of enol-**1a** and enol-**1b** were prepared through sublimation as follows: single bulk crystals were placed in a small glass dish covered with a silanated glass plate; the glass dish was placed in a large Petri dish on a heater at 140 °C (**1a**) or 150 °C (**1b**) for several hours (Fig. S7, ESI†). From among several dozens of crystals, the crystals with a size and shape suitable for mechanical bending observations were selected using an optical microscope. The face indices of the microcrystals were identified *via* powder X-ray diffraction measurements using a Smartlab system (Rigaku Corp., Tokyo, Japan) and a monochromatic Co K α radiation source ($\lambda = 1.78892$ Å).

Differential scanning calorimetry measurements

Differential scanning calorimetry profiles measurements were conducted using a differential scanning calorimeter (DSC 8500, PerkinElmer, Waltham, MA, USA) at a rate of 10 °C min⁻¹ for heating and cooling under N₂ gas at atmospheric pressure.

X-Ray crystallographic analyses

Single-crystal X-ray diffraction data for enol-**1a** and enol-**1b** were collected using an R-Axis RAPID-F instrument (Rigaku

Corp.) with monochromatic Mo-K α radiation ($\lambda = 0.71075$ Å). The initial structures were solved using direct methods in the SHELXT program⁵³ and refined on F^2 using full-matrix least-squares techniques in the SHELXL program.⁵⁴ Calculations were performed using the Rigaku CrystalStructure software package (Rigaku)⁵⁵ and the Olex2 graphical interface.⁵⁶ Unit cell parameters before and under UV laser irradiation (375 nm; 960 mW cm⁻², FOLS-03, Sawaki Kobo Co. Ltd, Shizuoka, Japan) were also measured using this diffractometer.

Ultraviolet-visible diffuse reflectance spectra

Ultraviolet-visible (UV-vis) diffuse reflectance spectra of powdered enol-**1a** and enol-**1b** crystals were measured using a spectrometer (Lambda 650; PerkinElmer). Powdered crystals were mounted on a glass plate and covered with a quartz glass plate. Each sample was irradiated with UV light-emitting diodes at 365 nm and 40 mW cm⁻² (UV-400, Keyence, Osaka, Japan) to determine its photoisomerisation properties. After the spectral change became saturated, the UV light was turned off and the sample was either kept in the dark or exposed to visible light (520 nm; 4.4 mW cm⁻²; FOLS-03, Sawaki Kobo) to clarify its thermal and photochemical back-isomerisation properties, respectively. All measurements were performed within a wavelength range of 200–800 nm at 1 nm resolution.

Mechanical bending observations

The mechanical bending of enol-**1a** and enol-**1b** crystals under UV light irradiation was recorded using a digital high-speed microscope at a frame rate of 30–1000 fps (VW-6000, Keyence). Irradiation was conducted using one UV and two visible light lasers (375, 520, and 450 nm, respectively; FOLS-03, Sawaki Kobo). For 375 and 520 nm lasers, the output laser beam was collimated using a collimator (F220FC-532, Thorlabs Inc., Newton, NJ, USA); the beam diameters were 3.0 mm (375 nm laser) and 3.5 mm (520 nm laser), respectively. Light irradiation was controlled using a microcontroller (UNO; Arduino, Somerville, MA, USA) as shown in Fig. S23 (ESI†). Movies were analysed using the Tracker Video Analysis and Modelling Tool⁵⁷ to extract the time dependence of the bend angle of the crystal tip. The definition of the bend angle is depicted in Fig. S24 (ESI†). Surface temperature distribution changes upon irradiation with light were monitored using an infrared thermography camera at a frame rate of 60 fps (FSV-2000, Apiste, Osaka, Japan). The time constants for bending/straightening and temperature increase/decrease were extracted by fitting their time dependence to a monoexponential curve. When a crystal showed two-step bending (Fig. 5e), the time dependence of the bend angle was fitted using a biexponential curve, where the fast and slow components were regarded as the contributions of the photothermal effect and photoisomerisation, respectively.

Results and discussion

Crystal structures

Single plate-like yellow crystals of enol-**1a** (Fig. 1a) and enol-**1b** (Fig. 1b) were readily obtained through the slow evaporation of



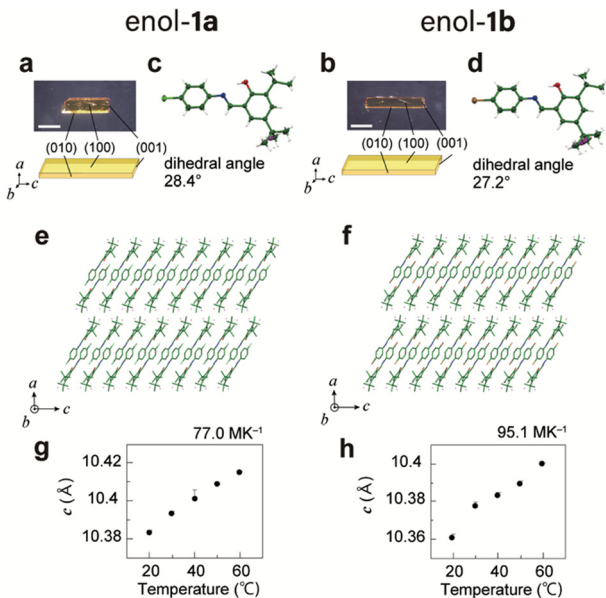


Fig. 1 Crystal structures of the enol-**1a** and enol-**1b** crystals. (a and b) Photographs and face indices of single plate-like (a) enol-**1a** and (b) enol-**1b** crystals. Scale bars, 1 mm. (c and d) Oak Ridge Thermal Ellipsoid Plot (ORTEP) drawings at 20 °C with a thermal ellipsoid of 25% probability. Disordered *tert*-butyl substituents are indicated in magenta. (e and f) Molecular packing on the (010) side face. (g and h) Temperature dependence of the length of the *c*-axis.

methanol solutions at room temperature. The melting points of enol-**1a** and enol-**1b** crystals were 153.5 °C and 162.1 °C, respectively. The differential scanning calorimetry profiles of both crystals showed no significant peaks other than their melting points, indicating that these crystals do not undergo thermal phase transitions and are stable over the temperature range of −50 °C to 150 °C (Fig. S1, ESI†). X-ray crystallographic analyses revealed that the structures of both crystals belonged to the monoclinic crystal system and space group $P2_1/c$ (Table S1, ESI†), which is consistent with previous reports.^{58–60} One independent molecule was found in an asymmetric unit, with dihedral angles between salicyl and phenyl rings of 28.4° (enol-**1a**, Fig. 1c) and 27.2° (enol-**1b**, Fig. 1d). The molecules in enol-**1a** and enol-**1b** crystals were connected by short CH/O and CH/ π contacts to form a one-dimensional motif along the *c*-axis, which corresponded to the longitudinal direction of the bulk crystals (Fig. 1e, f and Fig. S2, S3, ESI†). Molecular interactions along the *a*-axis (thickness direction) were weak because only van der Waals forces of the *tert*-butyl groups were present between adjacent one-dimensional motifs. The enol-**1a** and enol-**1b** crystals had nearly identical lattice parameters and molecular packing (Table S1, ESI†), indicating that these two compounds produced isomorphous crystals. The lengths of the *c*-axes increased in proportion to temperature, yielding thermal expansion coefficients of 77.0 and 95.1 MK^{−1} for enol-**1a** and enol-**1b** crystals, respectively (Fig. 1g, h and Fig. S4, ESI†).

Photoisomerisation

Under UV-light-emitting diode irradiation of the powder enol-**1a** and enol-**1b** crystals, the absorption at 400–600 nm

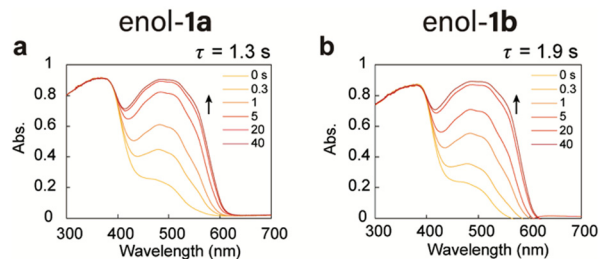


Fig. 2 Ultraviolet-visible (UV-vis) diffuse reflectance spectra of powder (a) enol-**1a** and (b) enol-**1b** crystals upon irradiation with a UV light-emitting diode (LED).

increased and reached a steady state within 40 s (Fig. 2a and b), accompanied by a colour change from yellow to red (Fig. S5, ESI†). Difference spectra before and under UV light irradiation showed a new absorption peak at 515 nm, which was derived from photoisomerisation from the enol to *trans*-keto form; this yielded apparent time constants (τ) of 1.3 s (**1a**) and 1.9 s (**1b**), respectively. After the removal of UV light, the new absorption band (400–600 nm) decreased slowly *via trans*-keto to enol thermal back-isomerisation; it reached the original state within 180 min, with time constants of 1.1 h (**1a**) and 1.2 h (**1b**), respectively (Fig. S6, ESI†). Immediately after the UV light was turned off, back-isomerisation was accelerated to 35.2 s (**1a**) and 76.0 s (**1b**) through visible light irradiation from photochemical back-isomerisation.

Crystal bending through photoisomerisation and the photothermal effect

When the (100) top face of a thin plate-like crystal of enol-**1a** (length: 385 μm , width: 30.0 μm , thickness: 3.8 μm) was irradiated with a UV laser (928 mW cm^{−2}) from the left (Fig. 3a), the crystal bent toward the light source to reach a maximum bend angle of 12.1° at 0.83 s; it then gradually returned to 9.5° at 8.1 s (Fig. 3b and Movie S1, ESI†). After removal of the laser, the crystal returned to its original straight shape at 8 s. The time profile of the bend angle was fitted using single-exponential equations, which yielded a bending time constant (τ_b) of 0.24 s and straightening time constant (τ_s) of 2.3 s (Fig. 3c). Next, the light intensity dependence of the bending motion was examined for another enol-**1a** crystal (1980 \times 67.5 \times 31.4 μm^3 ; Fig. 3d and Fig. S13, Movie S2, ESI†). The maximum bend angle linearly increased under weak UV light intensity and was saturated under strong UV irradiation (Fig. 3e); no clear correlation was observed between UV intensity and either τ_b or τ_s (Fig. 3f). In contrast, the straightening motion was considerably accelerated when visible light was applied (520 nm, Fig. 3g). The speed of thermal back-isomerisation of **1a** was increased under visible light application by photochemical back-isomerisation (Fig. S6, ESI†), indicating that the bending of thin crystals was caused by enol-keto photoisomerisation. The bending motion was repeatable; when alternating UV laser irradiation (5 s on/10 s off) was applied to another enol-**1a** crystal (2004 \times 92.2 \times 33.9 μm^3), the crystal bent and returned reversibly more than 100 times without deterioration, thus demonstrating excellent durability (Fig. S11, ESI†).





Fig. 3 Bending of thin enol-**1a** crystals ((A) $385 \times 30 \times 3.8 \mu\text{m}^3$, Movie S1, ESI†) (B) $1980 \times 67.5 \times 31.4 \mu\text{m}^3$, Movie S2, ESI†) by photoisomerisation upon UV laser irradiation. Photographs of the crystal (a) before and (b) under UV irradiation. Scale bars: $50 \mu\text{m}$. (c and d) Time profile of the bend angle. (e and f) UV light intensity dependence of the (e) maximum bend angle and (f) time constants for bending (solid circles) and straightening (open circles). (g) Visible light intensity dependence of the straightening time constant.

This bending toward a light source is attributed to the contraction of the top (100) face along the longitudinal direction (*c*-axis) in response to the enol–keto photoisomerisation of molecules. X-ray crystallographic analyses of enol-**1a** before and under UV light irradiation revealed slight but significant contraction of the length of the *c*-axis (Fig. S8, ESI†).

Next, upon UV laser irradiation of the (100) top surface of a thick enol-**1a** crystal ($2910 \times 331 \times 194 \mu\text{m}^3$, Fig. 4a), the crystal quickly bent -0.38° away from the light source at 0.06 s (Fig. 4b, d and Movie S3, ESI†). The crystal returned to its initial straight shape 0.12 s after the laser was turned off. The time constants τ_b and τ_s were 17 and 57 ms, respectively. The temperature of the irradiated top surface increased from 21.0°C to 50.2°C at 2 s ($\tau = 0.53$ s) after the light was turned off; it decreased to the initial temperature at 4 s ($\tau = 0.55$ s) after the light was turned off (Fig. 4c and d). The maximum bend angle and maximum top surface temperature linearly increased with increasing UV light intensity (Fig. 4e, g and Fig. S15, ESI†). At all UV intensities, τ_b and τ_s were one order of magnitude smaller than the time constants of the temperature increase and decrease (Fig. 4f and h), indicating that high-speed bending was caused by the photothermal effect; specifically, gradient thermal expansion along the length direction because of a non-steady temperature gradient in the thickness direction resulted in high-speed bending.⁴¹

When the (100) top face of a slightly thick enol-**1a** crystal ($3680 \times 300 \times 85.3 \mu\text{m}^3$, Fig. 5a) was exposed to the UV laser, it



Fig. 4 Bending of a thick enol-**1a** crystal ($2910 \times 331 \times 194 \mu\text{m}^3$) by the photothermal effect upon UV laser irradiation (Movie S3, ESI†). (a) Photograph of the crystal (side view). Scale bar: $500 \mu\text{m}$. (b and c) Sequential snapshots of the crystal taken in (b) side view using a digital microscope and (c) top view using an infrared thermography camera. (d) Time dependence of the bend angle (black) and maximum surface temperature (red). (e–h) UV laser intensity dependence of the (e) maximum bend angle, (f) time constants for bending (solid circles) and straightening (open circles), (g) maximum top surface temperature, and (h) time constants for temperature increase (solid circles) and decrease (open circles).

bent -0.23° away within 0.01 s ($\tau_b = 4.7$ ms) and then gradually bent $+0.15^\circ$ toward the irradiation direction by 5.0 s ($\tau_b = 0.69$ s) (Fig. 5b, e and Movie S4, ESI†). Subsequent removal of the laser caused the crystal to bend upward abruptly ($+0.42^\circ$) at 5.01 s ($\tau_s = 5.0$ ms); it gradually returned to its initial straight shape by 180 s ($\tau_s = 61.6$ s). The top surface temperature increased from 20.5°C to 37.6°C (Fig. 5c and e). A schematic diagram of a possible mechanism for this two-step bending is shown in Fig. 5d. Upon UV laser irradiation, the crystal bends away from the light source through the photothermal effect [Fig. 5d(ii)]. After the temperature gradient reaches the steady state, it bends toward the light source through enol–keto photoisomerisation of molecules near the irradiated surface [Fig. 5d(iii)]. After the light is turned off, the crystal bends further toward through relaxation of the photothermal effect [Fig. 5d(iv)] and is restored to its original shape *via* thermal back-isomerisation [Fig. 5d(v)].

The bend angle caused by photoisomerisation increased at weak UV light intensity and then decreased slightly under strong UV light irradiation (black solid circles, Fig. 5f). In contrast, the bend angle caused by the photothermal effect





Fig. 5 Bending of a slightly thick enol-**1a** crystal ($3680 \times 300 \times 85.3 \mu\text{m}^3$) through photoisomerisation and the photothermal effect (Movie S4, ESI†). (a) Side view of the crystal. Scale bar: $500 \mu\text{m}$. (b and c) Sequential snapshots of (b) the crystal tip (side view) and (c) temperature (top view). (d) Schematic illustration of a possible bending mechanism. (e) Time dependence of the bend angle (black) and maximum top surface temperature (red). (f–i) UV laser intensity dependence of the (f) maximum bend angle, (g) time constants for bending and straightening, (h) maximum top surface temperature (red solid circles) and temperature difference ΔT (red open circles), and (i) time constants for temperature increase (red solid circles) and decrease (red open circles). (f) Contributions of photoisomerisation (black solid circles) and the photothermal effect (red solid circles). (g) Time constants for bending (black solid circles) and straightening (black open circles) by photoisomerisation, and bending (red solid circles) and straightening (red open circles) by the photothermal effect.

linearly increased in proportion to UV laser intensity (red solid circles, Fig. 5f); similarly, the maximum top surface temperature linearly increased with increasing UV intensity (Fig. 5h and Fig. S14, ESI†). The time constants for bending and straightening by photoisomerisation decreased and increased, respectively, in proportion to UV intensity; the time constants obtained by the photothermal effect remained stable (Fig. 5g). The time constants for temperature increase and decrease were also stable as UV intensity changed (Fig. 5i).

The bending behaviour of enol-**1b** crystals upon UV laser irradiation was also examined (Fig. 6 and Fig. S17, S18, Movie S5, ESI†). A thin plate-like enol-**1b** crystal ($171 \times 17.2 \times 2.4 \mu\text{m}^3$) bent toward the irradiation direction through photoisomerisation (Fig. 6a). A slightly thick enol-**1b** crystal ($2410 \times 191 \times 65.5 \mu\text{m}^3$) exhibited two-step bending through photoisomerisation and the photothermal effect (Fig. 6b). A thick crystal ($2030 \times 344 \times 174 \mu\text{m}^3$) bent away quickly through the photothermal effect (Fig. 6c). These results demonstrate that isomorphic crystals of enol-**1a** and enol-**1b**—with similar molecular structures, crystal structures, and photoisomerisation properties—exhibit similar photomechanical actuation upon UV light irradiation.

Actuation switching by crystal thickness

As discussed above, thin crystals bent toward the light source through photoisomerisation (Fig. 3 and 6a), whereas thick

crystals bent away quickly through the photothermal effect (Fig. 4 and 6c). Slightly thick crystals exhibited two-step bending through photoisomerisation and the photothermal effect (Fig. 5 and 6b). The thickness dependence of the maximum bend angle of enol-**1a** crystals under UV laser irradiation is shown in Fig. 7a; detailed information concerning the crystal size and bending angles of all specimens is provided in Fig. S12 (ESI†). The bend angle caused by photoisomerisation decreased in proportion to crystal thickness, reaching zero at approximately $100 \mu\text{m}$ (Fig. S9, ESI†), because the strain generated by photoproducts near the irradiated surface was not effectively translated into macroscopic bending for thicker crystals. This threshold value ($100 \mu\text{m}$) for crystal actuation through photoisomerisation was higher than the threshold value ($40 \mu\text{m}$) of another salicylideneaniline derivative crystal with an *o*- NH_2 substituent.⁴¹ The Timoshenko bimetal model estimated the thickness of the photoreacted layer of enol-**1a** crystals to be $3.54 \mu\text{m}$ (Fig. S10, ESI†), which is larger than the $2.64 \mu\text{m}$ for the salicylideneaniline crystal with an *o*- NH_2 substituent⁴¹ and 1.0 – $2.0 \mu\text{m}$ for some diarylethene crystals.^{61,62} Thus, light is able to penetrate deep into the enol-**1a** crystals, resulting in the bending of slightly thick crystals through photoisomerisation. Photothermal effect-induced bending was observed in thick ($>33 \mu\text{m}$) crystals, presumably because sufficient size and thickness are required to form a temperature gradient along the thickness direction. The threshold thickness ($33 \mu\text{m}$) for crystal actuation through the





Fig. 6 Bending of enol-**1b** crystals (Movie S5, ESI†). (a) Thin ($171 \times 17.2 \times 2.4 \mu\text{m}^3$), (b) slightly thick ($2410 \times 191 \times 65.5 \mu\text{m}^3$), and (c) thick ($2030 \times 344 \times 174 \mu\text{m}^3$) crystals bent through photoisomerisation and/or the photothermal effect upon UV laser irradiation of the (100) top face at 960 mW cm^{-2} (a and b) and 230 mW cm^{-2} (c).

photothermal effect in this study was slightly higher than the threshold thickness ($20 \mu\text{m}$) reported in a previous study.⁴¹

The thickness dependence of the bending and straightening time constants of enol-**1a** crystals is shown in Fig. 7b; the time constants for photothermally induced bending ($\sim 0.01 \text{ s}$) were two orders of magnitude smaller (*i.e.*, faster) than the time constants for photoisomerisation-induced bending ($\sim 1 \text{ s}$), which is consistent with previous reports.^{41,50} These results suggest that the bending and straightening time constants may be used as indicators to distinguish photoisomerisation-driven bending ($\tau = \sim 1 \text{ s}$) from photothermal-driven bending ($\tau = \sim 0.01 \text{ s}$). Overall, these findings demonstrate that crystal bending direction and speed can be readily switched by altering crystal thickness.

Additionally, the length, width, and aspect ratio dependence on the bending behaviour was examined (Fig. S16, ESI†). The bend angle caused by photoisomerisation decreased in proportion to the length and width while increased in proportion to the aspect ratio. The bend angle caused by the photothermal effect showed no clear correlations with length and width but displayed a slight increase in proportion to the aspect ratio.

We also investigated the dependence of crystal actuation on the irradiated face (Fig. 8A, D and S19, ESI†). The thin enol-**1a**



Fig. 7 Thickness dependence of the (a) maximum bend angle and (b) time constants for the bending and straightening of enol-**1a** crystals upon UV laser irradiation.

crystal, which bent toward the irradiation direction through photoisomerisation (Fig. 3B and 8a), was rotated by 90° and set with its (010) side face facing upward. Upon UV irradiation of the side face from the top, the thin crystal exhibited two-step bending, such that it bent first quickly away and then slowly toward the UV source (Fig. 8j). These distinct bending motions depending on the irradiated face can be explained as follows. When the thin crystal is rotated by 90° , the length relative to the light penetration direction becomes larger ($67.5 \mu\text{m}$), exceeding the threshold ($> 33 \mu\text{m}$) for crystal actuation by the photothermal effect; this phenomenon results in actuation through both the photothermal effect and photoisomerisation (*i.e.*, two-step bending). Next, the slightly thick enol-**1a** crystal, which exhibited two-step bending through photoisomerisation and the photothermal effect (Fig. 5 and 8b), was rotated by 90° and irradiated with the UV laser. The slightly thick crystal exhibited one-step quick bending away, accompanied with a temperature increase on the top surface (Fig. 8k). This effect occurred because 90° rotation caused the length relative to the light penetration direction to become much larger ($300 \mu\text{m}$), prohibiting actuation through photoisomerisation ($< 100 \mu\text{m}$, Fig. 7a). Notably, the thick crystal bent away, regardless of the irradiated face, because of its large size (Fig. 8c and l).

Actuation switching by light wavelength

Considering that photoisomerisation is induced solely by UV light ($< 400 \text{ nm}$), whereas the photothermal effect can be





Fig. 8 Crystal actuation switching achieved by altering crystal thickness and light wavelength. Time dependence of the (a–l) bending and (b, c, e, f, h, i, k and l) irradiated surface temperature of enol-**1a** crystals of varying size and thickness (thin: $1980 \times 67.5 \times 31.4 \mu\text{m}^3$, slightly thick: $3680 \times 300 \times 85.3 \mu\text{m}^3$, thick: $2910 \times 331 \times 194 \mu\text{m}^3$; the same crystals are shown in Fig. 3B, 5, and 4, respectively) upon (A) UV laser (750 mW cm^{-2}) irradiation of the (100) top face, (B) simultaneous UV (750 mW cm^{-2}) and visible (520 nm ; 507 mW cm^{-2}) laser irradiation of the (100) top face, (C) visible laser (450 nm ; and (g and i) 1540 mW cm^{-2} ; spot diameter 2.0 mm and (h) 3620 mW cm^{-2} ; spot diameter 1.3 mm) irradiation of the (100) top face, and (D) UV laser (750 mW cm^{-2}) irradiation of the (010) side face. Numbers indicate the time constants for bending/straightening and temperature increase/decrease.



triggered by both UV light and visible light,⁴¹ further actuation switching could be achieved by changing the light wavelength (Fig. 8A–C and Fig. S20, S21, Movies S6, S7, ESI†). Upon simultaneous UV (375 nm) and visible (520 nm) laser irradiation of the thin enol-**1a** crystal, which bent toward UV light (Fig. 3B and 8a), the crystal did not clearly bend toward the light source (Fig. 8d) because back-isomerisation was accelerated under visible light; this suppressed any bending motion toward the light source because of photoisomerisation. Similarly, the thin crystal showed no significant bending toward the visible laser at 450 nm because visible light cannot induce photoisomerisation (Fig. 8g). Instead, the crystal bent very slightly (-0.018°) away from the visible laser, presumably because of the photothermal effect (Fig. 8g).

When the slightly thick crystal, which exhibited two-step bending through photoisomerisation and the photothermal effect under UV light (Fig. 5 and 8b), was simultaneously irradiated with UV (375 nm) and visible (520 nm) lasers, it exhibited one-step quick bending away through the photothermal effect; this was accompanied by a temperature increase at the top surface (Fig. 8e). This switching (from two-step bending to bending away) occurs because visible light accelerates back-isomerisation and suppresses photoisomerisation-driven bending, whereas visible light induces photothermally driven bending. Indeed, upon visible laser (450 nm) irradiation, the slightly thick crystal also bent away quickly through the photothermal effect; upon pulsed visible laser irradiation, it achieved 10 Hz high-speed bending (Fig. 8h and Fig. S22, Movie S8, ESI†). Notably, the thick crystal shown in Fig. 4 bent away, regardless of the light wavelength (Fig. 8c, f and i), because thick crystals are actuated by the photothermal effect, not by photoisomerisation. These results demonstrate that the actuation of thick and slightly thick crystals can be tuned by altering the light wavelength.

Conclusion

The photomechanical motions of the isomorphous crystals of two salicylideneaniline derivatives with 4-chloro (**1a**) and 4-bromo (**1b**) substituents in the enol form were examined based on photoisomerisation and the photothermal effect. Plate-like enol-**1a** and enol-**1b** crystals were readily obtained by the evaporation of methanol solutions at room temperature or by sublimation. Enol-**1a** and enol-**1b** crystals have similar crystalline structures, photoisomerisation properties, and mechanical motions under light irradiation. Under UV light irradiation of the (100) top face, thin ($<33\ \mu\text{m}$) crystals bent toward the light source because of photoisomerisation; this bending was attributed to local contraction of the irradiated top surface. Thick ($>100\ \mu\text{m}$) crystals bent away quickly through the photothermal effect; this rapid bending resulted from gradient thermal expansion along the thickness direction. Slightly thick ($33\text{--}100\ \mu\text{m}$) crystals exhibited two-step bending through both photoisomerisation and the photothermal effect. Upon UV light irradiation of the (010) side face, the bending motions of thin and slightly thick crystals switched to two-step

bending and bending away, respectively, because the length relative to the light penetration direction became larger as the crystals were rotated by 90° . Upon simultaneous UV and visible light irradiation or visible light irradiation alone, thin and slightly thick crystals changed their bending behaviour to no significant bending and bending away, respectively, because photoisomerisation was suppressed. These results demonstrate that crystal actuation (*i.e.*, bending direction and speed) can be readily switched by changing crystal thickness and light wavelength. We anticipate that these results will open new avenues for the design of crystal actuators with desired output; they will also expand the range of designs and applications of photo-mechanical crystals.

Conflicts of interest

There are no conflicts to declare.

Acknowledgements

This research was supported by JSPS Grant-in-Aid for Scientific Research B (17H03107) for H. K., JSPS Research Fellowship for Young Scientists (22J22384 and 21J20125) for S. H. and Y. H., respectively, and the Grant-in-Aid for Young Scientists (Early Bird) at Waseda Research Institute for Science and Engineering for S. H. and Y. H. S. H. and Y. H. thank the Graduate Program for Power Energy Professionals, Waseda University from MEXT WISE Program.

Notes and references

- 1 *Mechanically Responsive Materials for Soft Robotics*, ed. H. Koshima, Wiley-VCH, Weinheim, 2020.
- 2 H. Zeng, P. Wasylczyk, D. S. Wiersma and A. Priimagi, *Adv. Mater.*, 2018, **30**, 1703554.
- 3 Y. Chen, J. Yang, X. Zhang, Y. Feng, H. Zeng, L. Wang and W. Feng, *Mater. Horiz.*, 2021, **8**, 728–757.
- 4 Y. Yu, M. Nakano and T. Ikeda, *Nature*, 2003, **425**, 145.
- 5 T. White and D. Broer, *Nat. Mater.*, 2015, **14**, 1087–1098.
- 6 M. Irie, T. Fukaminato, K. Matsuda and S. Kobatake, *Chem. Rev.*, 2014, **114**, 12174–12277.
- 7 P. Naumov, S. Chizhik, M. K. Panda, N. K. Nath and E. Boldyreva, *Chem. Rev.*, 2015, **115**, 12440–12490.
- 8 P. Naumov, D. P. Karothu, E. Ahmed, L. Catalano, P. Commins, J. M. Halabi, M. B. Al-Handawi and L. Li, *J. Am. Chem. Soc.*, 2020, **142**, 13256–13272.
- 9 H. Koshima, S. Hasebe, Y. Hagiwara and T. Asahi, *Isr. J. Chem.*, 2021, **61**, 683–696.
- 10 M. Irie, *Diarylethene Molecular Photoswitches*, Wiley-VCH, Weinheim, 2021.
- 11 Y. Yang, H. Hao and C. Xie, *CrystEngComm*, 2022, **24**, 3136–3149.
- 12 G. A. Abakumov and V. I. Nevodchikov, *Dokl. Phys. Chem.*, 1982, **266**, 1407–1410.



- 13 E. V. Boldyreva, A. A. Sidelnikov, A. P. Chupakhin, N. Z. Lyakhov and V. V. Boldyrev, *Dokl. Phys. Chem.*, 1984, **277**, 893–896.
- 14 S. Kobatake, S. Takami, H. Muto, T. Ishikawa and M. Irie, *Nature*, 2007, **446**, 778–781.
- 15 H. Koshima, N. Ojima and H. Uchimoto, *J. Am. Chem. Soc.*, 2009, **131**, 6890–6891.
- 16 M. Morimoto and M. Irie, *J. Am. Chem. Soc.*, 2010, **132**, 14172–14178.
- 17 H. Koshima, K. Takechi, H. Uchimoto, M. Shiro and D. Hashizume, *Chem. Commun.*, 2011, **47**, 11423–11425.
- 18 F. Terao, M. Morimoto and M. Irie, *Angew. Chem., Int. Ed.*, 2012, **51**, 901–904.
- 19 H. Koshima, H. Nakaya, H. Uchimoto and N. Ojima, *Chem. Lett.*, 2012, **41**, 107–109.
- 20 O. S. Bushuyev, T. A. Singleton and C. J. Barrett, *Adv. Mater.*, 2013, **25**, 1796–1800.
- 21 H. Koshima, R. Matsuo, M. Matsudomi, Y. Uemura and M. Shiro, *Cryst. Growth Des.*, 2013, **13**, 4330–4337.
- 22 N. K. Nath, L. Pejov, S. M. Nichols, C. Hu, N. Saleh, B. Kahr and P. Naumov, *J. Am. Chem. Soc.*, 2014, **136**, 2757–2766.
- 23 T. Kim, L. Zhu, L. J. Mueller and C. J. Bardeen, *J. Am. Chem. Soc.*, 2014, **136**, 6617–6625.
- 24 S. Chizhik, A. Sidelnikov, B. Zakharov, P. Naumov and E. Boldyreva, *Chem. Sci.*, 2018, **9**, 2319–2335.
- 25 R. Kajiya, S. Sakakibara, H. Ikawa, K. Higashiguchi, K. Matsuda, H. Wada, K. Kuroda and A. Shimojima, *Chem. Mater.*, 2019, **31**, 9372–9378.
- 26 P. Gupta, T. Panda, S. Allu, S. Borah, A. Baishya, A. Gunnam, A. Nangiam, P. Naumov and N. K. Nath, *Cryst. Growth Des.*, 2019, **19**, 3039–3044.
- 27 J. M. Halabi, E. Ahmed, S. Sofela and P. Naumov, *Proc. Natl. Acad. Sci. U. S. A.*, 2021, **118**, e2020604118.
- 28 K. Ishizaki, R. Sugimoto, Y. Hagiwara, H. Koshima, T. Taniguchi and T. Asahi, *CrystEngComm*, 2021, **23**, 5839–5847.
- 29 L. Zhu, R. O. Al-Kaysi and C. J. Bardeen, *J. Am. Chem. Soc.*, 2011, **133**, 12569–12575.
- 30 D. Kitagawa, H. Nishi and S. Kobatake, *Angew. Chem., Int. Ed.*, 2013, **52**, 9320–9322.
- 31 T. Taniguchi, J. Fujisawa, M. Shiro, H. Koshima and T. Asahi, *Chem. – Eur. J.*, 2016, **22**, 7950–7958.
- 32 A. Takanabe, M. Tanaka, K. Johmoto, H. Uekusa, T. Mori, H. Koshima and T. Asahi, *J. Am. Chem. Soc.*, 2016, **138**, 15066–15077.
- 33 T. Kim, M. K. Al-Muhanna, S. D. Al-Suwaidan, R. O. Al-Kaysi and C. J. Bardeen, *Angew. Chem., Int. Ed.*, 2013, **52**, 6889–6893.
- 34 L. Zhu, R. O. Al-Kaysi and C. J. Bardeen, *Angew. Chem., Int. Ed.*, 2016, **55**, 7073–7076.
- 35 R. Wei, Y. Wang, N. Wang, Y. Hao, X. Huang, T. Wang and H. Hao, *Cryst. Growth Des.*, 2021, **21**, 3936–3946.
- 36 F. Tong, M. Al-Haidar, L. Zhu, R. O. Al-Kaysi and C. J. Bardeen, *Chem. Commun.*, 2019, **55**, 3709.
- 37 M. Tamaoki, D. Kitagawa and S. Kobatake, *Cryst. Growth Des.*, 2021, **21**, 3093–3099.
- 38 P. Naumov, S. C. Sahoo, B. A. Zakharov and E. V. Boldyreva, *Angew. Chem., Int. Ed.*, 2013, **52**, 9990–9995.
- 39 K. Kato, T. Seki and H. Ito, *Inorg. Chem.*, 2021, **60**, 10849–10856.
- 40 Y. Hagiwara, T. Taniguchi, T. Asahi and H. Koshima, *J. Mater. Chem. C*, 2020, **8**, 4876–4884.
- 41 S. Hasebe, Y. Hagiwara, J. Komiyama, M. Ryu, H. Fujisawa, J. Morikawa, T. Katayama, D. Yamanaka, A. Furube, H. Sato, T. Asahi and H. Koshima, *J. Am. Chem. Soc.*, 2021, **143**, 8866–8877.
- 42 S. Mittapalli, D. S. Perumalla and A. Nangia, *IUCr*, 2017, **4**, 243–250.
- 43 L. Gao, Y. Hao, X. Zhang, X. Huang, T. Wang and H. Hao, *CrystEngComm*, 2020, **22**, 3279–3286.
- 44 Y. Hao, L. Gao, X. Zhang, L. Wei, T. Wang, N. Wang, X. Huang, H. Yu and H. Hao, *J. Mater. Chem. C*, 2021, **9**, 8294–8301.
- 45 D. Kitagawa, K. Kawasaki, R. Tanaka and S. Kobatake, *Chem. Mater.*, 2017, **29**, 7524–7532.
- 46 Y. Hao, S. Huang, Y. Guo, L. Zhou, H. Hao, C. J. Barrett and H. Yu, *J. Mater. Chem. C*, 2019, **7**, 503–508.
- 47 T. Taniguchi, H. Sato, Y. Hagiwara, T. Asahi and H. Koshima, *Commun. Chem.*, 2019, **2**, 19.
- 48 A. Fujimoto, N. Fujinaga, R. Nishimura, E. Hatano, L. Kono, A. Nagai, A. Sekine, Y. Hattori, Y. Kojima, N. Yasuda, M. Morimoto, S. Yokojima, S. Nakamura, B. L. Feringa and K. Uchida, *Chem. Sci.*, 2020, **11**, 12307–12315.
- 49 B. B. Rath, M. Gupta and J. J. Vittal, *Chem. Mater.*, 2022, **34**, 178–185.
- 50 S. Hasebe, Y. Hagiwara, K. Takechi, T. Katayama, A. Furube, T. Asahi and H. Koshima, *Chem. Mater.*, 2022, **34**, 1315–1324.
- 51 D. Kitagawa, H. Tsujioka, F. Tong, X. Dong, C. J. Bardeen and S. Kobatake, *J. Am. Chem. Soc.*, 2018, **140**, 4208–4212.
- 52 T. Kawato, H. Koyama, H. Kanatomi, H. Tagawa and K. Iga, *J. Photochem. Photobiol., A*, 1994, **78**, 71–77.
- 53 G. M. Sheldrick, *Acta Crystallogr., Sect. A: Found. Adv.*, 2015, **71**, 3–8.
- 54 G. M. Sheldrick, *Acta Crystallogr., Sect. C: Struct. Chem.*, 2015, **71**, 3–8.
- 55 *CrystalStructure, version 4.2.2.*, Rigaku Corporation, Tokyo, Japan, 2016.
- 56 O. V. Dolomanov, L. J. Bourhis, R. J. Gildea, J. A. K. Howard and H. Puschmann, *J. Appl. Cryst.*, 2009, **42**, 339–341.
- 57 D. Brown, *Tracker Video Analysis and Modeling Tool, version 5.1.2.*, Cabrillo College, Aptos, California, USA, 2019.
- 58 J. Li, R. Zhao and C. Ma, *Acta Crystallogr., Sect. E: Crystallogr. Commun.*, 2007, **63**, o4923.
- 59 K. Johmoto, T. Ishida, A. Sekine, H. Uekusa and Y. Ohashi, *Acta Crystallogr., Sect. B: Struct. Sci.*, 2012, **68**, 297–304.
- 60 H. E. Mason, J. A. K. Howard and H. A. Sparks, *Acta Crystallogr., Sect. C: Struct. Chem.*, 2021, **77**, 659–667.
- 61 D. Kitagawa and S. Kobatake, *J. Phys. Chem. C*, 2013, **117**, 20887–20892.
- 62 D. Kitagawa, C. Iwaihara, H. Nishi and S. Kobatake, *Crystals*, 2015, **5**, 551–561.

